Oct 17th, 12:00 AM

Local Buckling Tests on Cold-formed Steel Beams

Cheng Yu

Benjamin W. Schafer

Sixteenth International Specialty Conference on Cold-Formed Steel Structures
Orlando, Florida USA, October 17-18, 2002

Local Buckling Tests on Cold-Formed Steel Beams

Cheng Yu[1], Benjamin W. Schafer[2]

Abstract

C- and Z-sections are two of the most common cold-formed steel shapes in use today. Accurate prediction of the bending performance of these sections is important for reliable and efficient cold-formed steel structures. Recent analytical work has highlighted discontinuities and inconsistencies in the AISI (1996) design provisions for stiffened elements under a stress gradient (i.e., the web of C- or Z-sections). New methods have been proposed for design, and an interim method has been adopted in the NAS (North American Specification 2001). However, existing tests on Cs and Zs do not provide a definitive evaluation of the design expressions, due primarily to incomplete restriction of the distortional buckling mode. Described in this paper are a series of flexural tests with details selected specifically to insure that local buckling is free to form, but distortional buckling and lateral-torsional buckling are restricted. The members selected for the tests provide systematic variation in the web slenderness (h/t) while varying other relevant non-dimensional parameters (i.e., h/b, b/t, d/t, d/b). Initial analysis of the completed testing indicates that overall test-to-predicted ratios for AISI (1996), S136 (1994), NAS (2001) and the Direct Strength Method (Schafer 2002) are all adequate, but systematic error is observed in AISI and S136 due to web/flange interaction.

Introduction

Determination of the ultimate bending capacity of cold-formed steel C- and Z-sections is complicated by yielding and the potential for local, distortional, and lateral-torsional buckling of the section (Figure 1). Local buckling is particularly prevalent and is characterized by the relatively short wavelength buckling of individual plate elements. Distortional buckling involves both translation and rotation at the compression flange/lip fold line of the member. It takes place as a consequence of distortion of a portion of the cross-section and predominately rigid response of a second portion (i.e. the flange/lip). The wavelength of distortional buckling is generally intermediate between that of local buckling and lateral-torsional buckling. Lateral-torsional buckling, or "global buckling," occurs when the cross-section buckles without distortion.

In Table 1 available experimental data is compared with the C- and Z-sections typically used in industry. A compilation of industry tests on purlins was reported by Elhouar and Murray (1985). This database of tests covers member geometries consistent with those used as purlins for metal building systems; however, the tested sections do not cover Z members reported by LGSI, nor the wider class of members reported in other industries. A large compilation of experimental data on Cs and Zs in flexure was summarized in

1. Graduate Research Assistant, Johns Hopkins University (cheng.yu@jhu.edu)
2. Assistant Professor, Johns Hopkins University (schafer@jhu.edu)

Schafer and Peköz (1999). This database covers a broad range of geometric ratios, but does not include members with web height to flange width ratio (h/b) near 1.0.

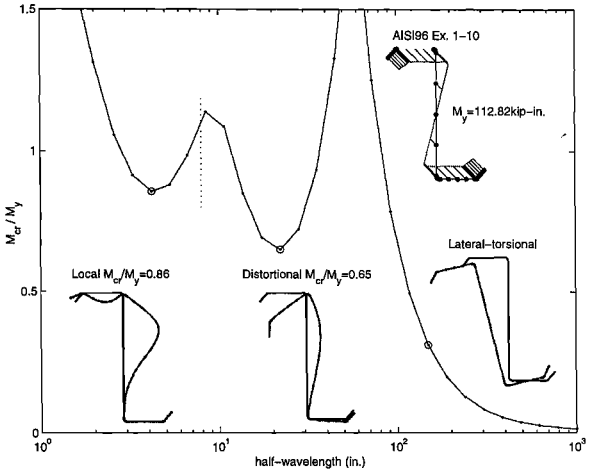

Figure 1 Buckling modes of the cold-formed steel beam

Existing tests on C- and Z-Sections generally focus on the performance of the compression flange and do not provide definitive evaluations of the design expressions for the web, due to: incomplete restriction of the distortional mode, arrangement of the specimens (back-to-back vs. toe- to-toe), and a general lack of information on bracing details. A series of new flexural tests focused on the role of web slenderness in local buckling failures of C- and Z-Sections are reported in this paper. Bracing has been carefully considered in these tests to insure that distortional buckling and lateral-torsional buckling do not influence the interpretation of results. The test results can be used for evaluation of existing and proposed methods for strength prediction of webs in local buckling. In addition, these tests can form the basis for later evaluations in which restrictions on the distortional mode are relieved.

Table 1 Range of geometry for industry members and available experimental data

		h/t		b/t		d/t		h/b		d/b	
		min	max	min	max	Min	max	min	max	min	max
Typical industry members	MBMA Z's	53	170	17	47	5	17	3.1	3.7	0.28	0.45
	SSMA members	25	318	11	132	1	33	1.0	10.9	0.12	0.33
	Rack members	23	136	16	45	6	15	1.0	3.2	0.27	0.38
Available experimental data	Elhouar & Murray (1985)	68	165	24	52	3	24	2.6	3.8	0.09	0.49
	Schafer & Peköz (1999)	43	270	15	75	3	34	1.5	13.7	0.14	0.70

Local Buckling Tests

Specimen Selection

The AISI (1996) Specification calculates the effective width of webs as a function of the web slenderness (h/t) alone. The proposed tests are designed to provide systematic variation in h/t while also varying the other non-dimensional parameters: web height vs. flange width ratio h/b, flange width vs. thickness ratio b/t, edge stiffener length vs. thickness ratio d/t, and edge stiffener vs. flange width ratio d/b, enough to determine the adequacy of existing and proposed design rules. The focus of the testing is on the webs, therefore significant variation in d/b is not investigated.

The primary consideration in investigating the web slenderness (h/t) is whether to achieve this variation by varying t, while holding h, b, d approximately constant or varying h while holding b, d and t approximately constant. Using industry standard sections dictates that studies on the Z-sections vary t, while holding h, b, and d approximately constant. However, the wide variety of C specimens commonly produced (SSMA standard sections, Table 1) allows both methods of variation to be examined for Cs.

Specimen dimensions

The dimensions of the specimens were recorded at the center of the specimen (mid-length) and mid-distance between the center and loading points (a total of three measurement locations for each specimen). The mean specimen dimensions, as determined from the three sets of measurements within the constant moment region are given in Table 2. The variables used for the dimensions are defined as follows:

h	out-to-out web depth
b_c	out-to-out compression flange width
d_c	out-to-out compression flange lip stiffener length
θ_c	compression flange stiffener angle from horizontal
b_t	out-to-out tension flange width
d_t	out-to-out compression flange lip stiffener length
θ_t	tension flange stiffener angle from horizontal
r_{hc}	outer radius between web and compression flange
r_{dc}	outer radius between compression flange and lip
r_{ht}	outer radius between web and tension flange
r_{dt}	outer radius between tension flange and lip

The variables used for the metal properties are defined as follows:

t	base metal thickness
f_y	yield stress
E	modulus of elasticity

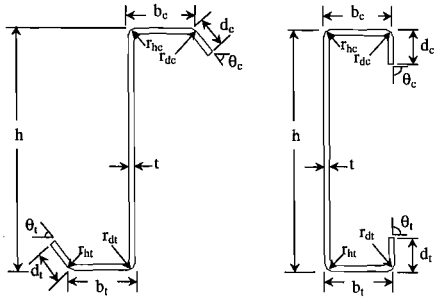

Figure 2 Definitions of specimen dimensions for Z and C

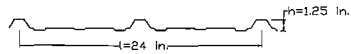

Figure 3 Dimension of panel

Testing Details

The basic testing setup is illustrated in Figure 4 through Figure 7. The 16 ft. span length, four-point bending test, consists of a pair of 18 ft. long C or Z specimens in parallel loaded at the ⅓ points. The members are oriented in an opposed fashion; such that in-plane rotation of the Cs or Zs lead to tension in the panel, and thus provide additional restriction against distortional buckling of the compression flange. Small angles (1¼ × 1¼ × 0.057 in.) are attached to the tension flanges every 12 in. and a through-fastened panel (t = 0.019 in., 1¼ in. high ribs, Figure 3) is attached to the compression flanges. Hot-rolled tube sections (10 × 7½ × 6 × ¼ in) bolt the pair of C or Z members together at the load points and the supports, and insure shear and web crippling problems are avoided at these locations. When testing the Cs, the hot-rolled angles detailed in Figure 6 connect to the tube and the end plate on the inside of the tube, instead of the outside of the tube, as detailed for the Z specimens.

After initial testing the details were improved to insure pure bending was maintained, and to restrict distortional and lateral-torsional buckling. Major improvements were made on the panel-to-purlin fastener configuration (see detail in subsequent section). The arrangement of rollers at the supports was modified to more closely model a pin-roller configuration (Figure 9). Additional web stiffening bars were added to the I-beams at the supports and load points. Machined, quarter-round aluminum blocks were placed as guides for the rollers at the loading points (Figure 10). Thin Teflon sheets were added at the load points and support points to limit unwanted friction and help insure the boundary conditions were predictable (Figure 9and Figure 10).

Table 2 Measured Geometry

Test label	Specimen	h	b_c	d_c	θ_c	b_t	d_t	θ_t	r_{htc}	r_{dc}	r_{ht}	r_{dt}	t	f_y
8.5Z120-3E2W	8.5Z120-3	8.44	2.58	0.96	47.2	2.46	0.99	48.9	0.36	0.36	0.35	0.35	0.1183	61.3
	8.5Z120-2	8.47	2.59	0.96	47.8	2.46	1.00	48.9	0.36	0.36	0.34	0.34	0.1180	60.1
8.5Z105-2E1W	8.5Z105-2	8.48	2.66	0.95	50.5	2.36	0.95	48.7	0.32	0.32	0.34	0.34	0.1040	68.8
	8.5Z105-1	8.42	2.69	0.97	50.7	2.36	0.91	48.7	0.31	0.31	0.34	0.34	0.1050	66.8
8.5Z092-4E2W	8.5Z092-4	8.41	2.61	0.93	53.0	2.41	0.96	50.8	0.29	0.29	0.31	0.31	0.0900	57.3
	8.5Z092-2	8.43	2.61	0.92	51.8	2.40	0.95	50.4	0.28	0.28	0.31	0.31	0.0887	57.0
8.5Z082-1E2W	8.5Z082-1	8.46	2.50	0.95	49.0	2.36	0.97	50.3	0.28	0.28	0.30	0.30	0.0801	58.4
	8.5Z082-2	8.45	2.51	0.95	47.9	2.40	0.95	52.4	0.28	0.28	0.30	0.30	0.0804	58.1
8.5Z073-6E5W	8.5Z073-6	8.50	2.52	0.92	49.6	2.40	0.94	50.9	0.28	0.28	0.30	0.30	0.0720	54.0
	8.5Z073-5	8.50	2.52	0.92	49.6	2.40	0.94	50.9	0.28	0.28	0.30	0.30	0.0727	55.6
8.5Z073-4E3W	8.5Z073-4	8.51	2.53	0.93	49.6	2.41	0.92	50.3	0.28	0.28	0.29	0.29	0.0715	56.1
	8.5Z073-3	8.50	2.53	0.91	50.1	2.38	0.96	51.0	0.28	0.28	0.30	0.30	0.0720	55.6
8.5Z073-1E2W	8.5Z073-2	8.50	2.54	0.93	50.2	2.41	0.92	51.0	0.28	0.28	0.30	0.30	0.0715	55.7
	8.5Z073-1	8.49	2.50	0.92	48.4	2.41	0.95	51.2	0.28	0.28	0.30	0.30	0.0720	54.8
8.5Z065-3E1W	8.5Z065-3	8.47	2.42	0.83	47.3	2.43	0.79	47.3	0.27	0.27	0.28	0.28	0.0640	53.5
	8.5Z065-1	8.47	2.44	0.76	47.4	2.43	0.84	47.1	0.28	0.28	0.27	0.27	0.0640	53.1
8.5Z059-4E3W	8.5Z059-4	8.50	2.50	0.77	50.9	2.35	0.72	48.9	0.28	0.28	0.28	0.28	0.0590	58.6
	8.5Z059-3	8.50	2.44	0.78	50.2	2.22	0.69	50.4	0.28	0.28	0.28	0.28	0.0595	58.5
8.5Z059-2E1W	8.5Z059-2	8.49	2.51	0.78	50.6	2.33	0.70	50.2	0.28	0.28	0.28	0.28	0.0590	59.1
	8.5Z059-1	8.50	2.51	0.78	51.2	2.33	0.71	49.4	0.28	0.28	0.28	0.28	0.0590	58.9
8C097-2E3W	8C097-2	8.04	2.12	0.57	85.6	2.08	0.52	85.7	0.30	0.28	0.28	0.30	0.0980	59.9
	8C097-3	8.03	2.09	0.56	84.0	2.08	0.54	88.2	0.30	0.28	0.28	0.29	0.0940	59.6
8C068-4E5W	8C068-4	8.03	2.03	0.52	83.2	2.04	0.53	87.0	0.28	0.25	0.24	0.24	0.0750	48.6
	8C068-5	8.01	2.05	0.52	84.0	2.04	0.54	87.6	0.27	0.26	0.24	0.27	0.0770	53.1
8C068-1E2W	8C068-2	8.02	2.04	0.52	83.4	2.04	0.53	87.6	0.28	0.25	0.24	0.26	0.0758	51.7
	8C068-1	8.03	2.03	0.53	83.1	2.05	0.53	88.1	0.30	0.26	0.25	0.26	0.0754	51.4
8C054-1E8W	8C054-1	8.00	2.04	0.52	88.9	2.07	0.50	84.7	0.22	0.23	0.23	0.23	0.0550	40.0
	8C054-8	8.08	2.02	0.58	88.1	1.96	0.48	82.3	0.22	0.20	0.22	0.23	0.0540	40.3
8C043-5E6W	8C043-5	8.04	2.02	0.53	88.8	1.98	0.53	87.3	0.18	0.20	0.21	0.20	0.0496	44.9
	8C043-6	8.06	2.01	0.53	88.9	2.00	0.46	87.0	0.19	0.20	0.22	0.20	0.0490	45.0
8C043-3E1W	8C043-3	8.04	2.02	0.54	89.3	2.01	0.53	87.5	0.19	0.19	0.19	0.19	0.0474	46.0
	8C043-1	8.03	2.02	0.54	89.0	1.98	0.54	85.8	0.19	0.19	0.29	0.19	0.0476	45.7
12C068-9E5W	12C068-9	12.02	1.92	0.53	82.0	2.00	0.55	85.3	0.28	0.27	0.30	0.28	0.0652	35.1
	12C068-5	12.00	1.79	0.55	85.9	2.06	0.53	94.8	0.27	0.27	0.22	0.27	0.0654	35.0
12C068-3E4W	12C068-3	11.97	1.96	0.59	82.5	1.99	0.56	77.4	0.26	0.27	0.27	0.27	0.0671	56.6
	12C068-4	12.02	2.01	0.52	80.6	2.00	0.52	83.3	0.26	0.27	0.26	0.27	0.0670	57.3
10C068-2E1W	10C068-2	10.08	1.93	0.50	83.2	1.98	0.52	83.3	0.27	0.25	0.27	0.25	0.0572	33.6
	10C068-1	10.03	2.04	0.55	80.7	1.97	0.54	81.9	0.27	0.26	0.28	0.25	0.0573	34.2
6C054-2E1W	6C054-2	6.04	2.00	0.56	85.7	2.00	0.52	90.0	0.21	0.24	0.26	0.25	0.0616	36.1
	6C054-1	6.03	2.01	0.56	86.5	2.05	0.52	90.5	0.22	0.25	0.25	0.24	0.0616	37.0
4C054-1E2W	4C054-1	3.95	1.99	0.55	79.2	2.02	0.55	77.4	0.24	0.24	0.23	0.24	0.0551	45.0
	4C054-2	3.96	1.95	0.50	74.2	1.96	0.55	74.8	0.22	0.27	0.25	0.25	0.0561	44.7
3.62C054-1E2W	3.62C054-1	3.65	1.97	0.49	77.1	2.00	0.42	88.1	0.23	0.26	0.26	0.25	0.0555	32.8
	3.62C054-2	3.67	1.99	0.51	79.8	1.97	0.44	79.8	0.24	0.25	0.26	0.26	0.0554	32.0
11.5Z092-1E2W	11.5Z092-1	11.41	3.33	0.96	50.1	3.51	0.96	49.5	0.25	0.27	0.27	0.27	0.1027	61.0
	11.5Z092-2	11.34	3.33	0.98	48.3	3.54	0.89	48.1	0.28	0.27	0.28	0.28	0.1033	60.4
11.5Z082-2E1W	11.5Z082-2	11.45	3.50	0.88	50.3	3.45	0.87	52.2	0.31	0.31	0.35	0.35	0.0837	61.5
	11.5Z082-1	11.47	3.49	0.90	50.6	3.43	0.88	51.0	0.32	0.32	0.35	0.35	0.0839	60.4
11.5Z073-2E1W	11.5Z073-2	11.39	3.51	0.87	46.0	3.35	0.83	44.8	0.27	0.28	0.27	0.28	0.0709	65.4
	11.5Z073-1	11.35	3.52	0.95	45.4	3.40	0.90	44.2	0.27	0.11	0.27	0.07	0.0695	66.8

Note:
Typical specimen label is xZ(or C)xxx-x. For example, 8.5Z073-1 means the specimen is 8.5 in. high for the web, Z-section, 0.073in. thick and the beam number is 1 (used to distinguish with other specimens with same dimensions). Typical test label is xZ(or C)xxx-xExW. For example, test 8.5Z073-1E2W means the two paired specimens are 8.5Z073-1 at the east side and 8.5Z073-2 at the west side.

The loading system employs a 20 kip MTS actuator, which has a maximum 6 in. stroke. The test is performed in displacement control at a rate of 0.0015 in./sec. A MTS 407 controller and load cell monitors the force and insures the desired displacement control is met. Meanwhile, deflections for one specimen at the ⅓ points were measured using two LVDTs (later, for the 10 in. C and 11.5 in. Z beam tests the 2 LVDTs were replaced by 4 position transducers). For a limited number of tests, strain gages were placed at mid-span, on the lip and the top of the web, at the same vertical cross-section height, to monitor the longitudinal strain. A Labview program was written to control the actuator as well as monitor and record the test data (Figure 8).

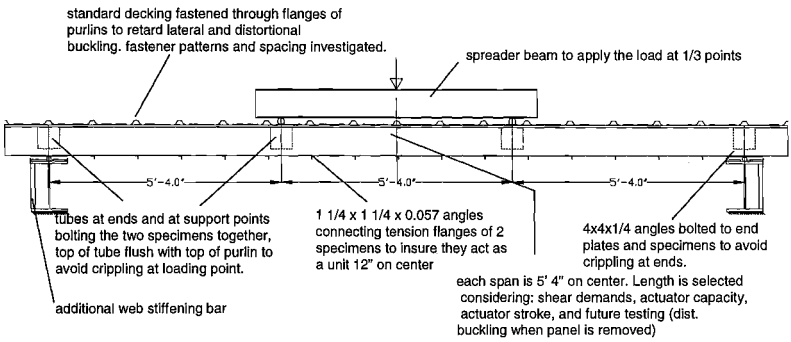

Figure 4 Elevation view of overall test arrangement for four point bending test

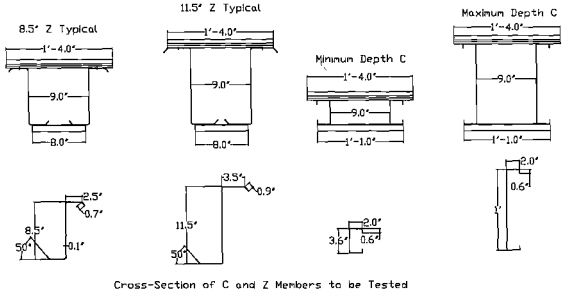

Figure 5 Range of tested specimens

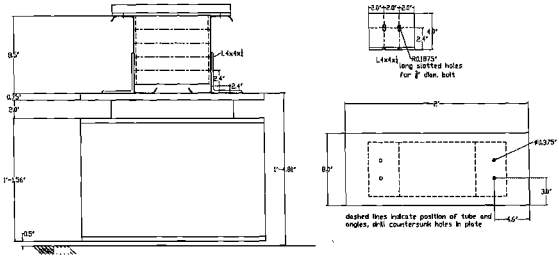

Figure 6 End-on elevation view of specimen at end support

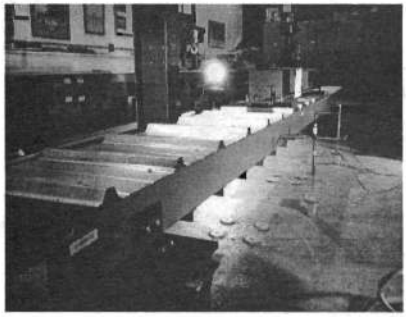

Figure 7 Overall view of test setup

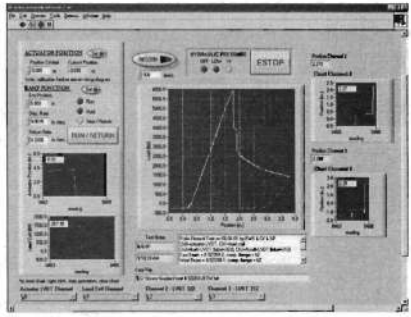

Figure 8 Labview program interface

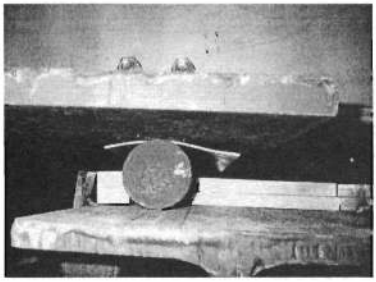

Figure 9 Support configuration

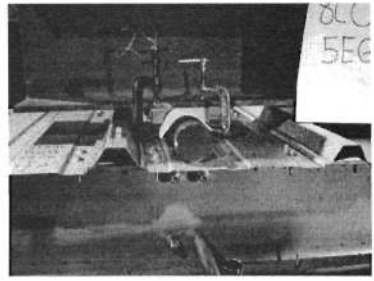

Figure 10 Loading point configuration

Panel-to-Purlin Fastener Configuration

A series of tests on the 8.5 in. deep Zs with t = 0.073 in. was conducted in order to determine the appropriate panel-to-purlin fastener detail for restricting the distortional mode. Initial testing using single panel-to-purlin fasteners placed through the center of the purlin flange and spaced at 12 in. o.c. failed at a capacity of 89% of the AISI prediction and visually appeared to suffer from deformations consistent with distortional buckling. Elastic finite element analysis (Figure 11) indicated that the lowest elastic buckling mode for this fastener detail was distortional buckling. Additional analysis indicated that a pair of fasteners placed on either side of the raised ribs of the panel (Figure 12 and Figure 13) would cause local buckling to be the lowest mode. Testing confirmed this prediction; paired fasteners as shown in Figure 13 provided a capacity 10% greater than single fasteners and 98% of the AISI (1996) prediction. Fasteners in the center of the panel pans did not further improve the results. Additionally, modeling indicates that the paired fasteners do not change the local buckling mode; thus, it can be safely assumed that this configuration restricts distortional buckling without artificially increasing the local buckling strength.

The selected standard panel-to-purlin fastener detail is a pair of screws placed 1.5 in. (2.5 in. for Z-section) apart and spaced 8 in. away from a second pair in the pan of the deck,

as show in Figure 13. The paired fastener configuration is only maintained inside the constant moment region of the test. In the shear span, one screw is used instead of one pair at the same location as that of the constant moment region.

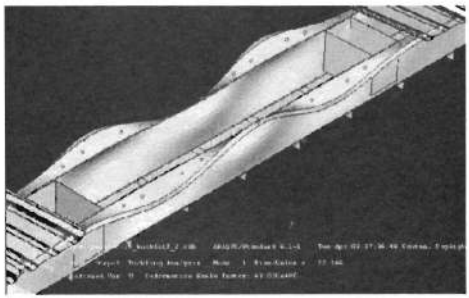

Figure 11 Lowest buckling mode predicted by FE model for single screw fastener configuration (note center panels removed for visual clarity only, red dots indicate fastener locations.)

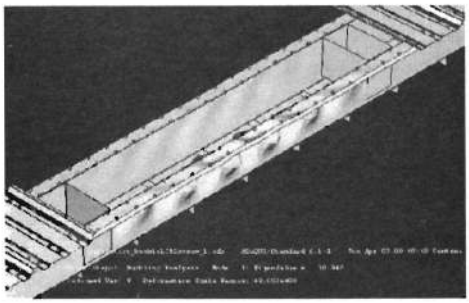

Figure 12 Lowest buckling mode predicted by FE model for paired screw fastener configuration (note center panels removed for visual clarity only, red dots indicate fastener locations.)

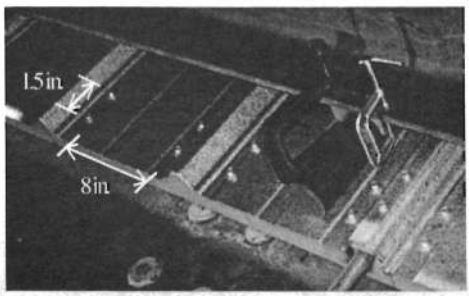

Figure 13 Selected standard panel-to-purlin and panel-to-panel fastener configuration (C-section)

Tension Tests

Tension tests were carried out following "ASTM E8–00 Standard Test Methods for Tension Testing of Metallic Material." The dimensions of a typical tensile coupon are shown in Figure 15. Three tensile coupons were taken from the end of each specimen: one from the web flat, one from the compression flange flat, and one from the tension flange flat. A screw-driven ATS 900; with a maximum capacity of 10 kips was used for the loading. An MTS 634.11E-54 extensometer was employed to monitor the deformation (Figure 14). Strain gages were installed on selected tensile coupons at the center, and on both sides, to verify the modulus of elasticity, E.

Two methods for yield strength determination were employed: 1) 0.2% Offset Method for the continuous yielding materials (Figure 16a); and 2) Auto Graphic Diagram Method for the materials exhibiting discontinuous yielding (Figure 16b).

The yield stress (f_y) can vary greatly from thickness to thickness. The large variation in f_y complicates comparisons across the test database, but it is important to recognize this variation, as f_y for the Zs varies from 53 to 69 ksi and for the Cs from 32 to 60 ksi. An E of 29500 ksi is assumed for all of the members. This is supported by limited testing on 0.059 in. and 0.082 in. tensile specimens from the Zs, which had an average measured E of 29200 ksi.

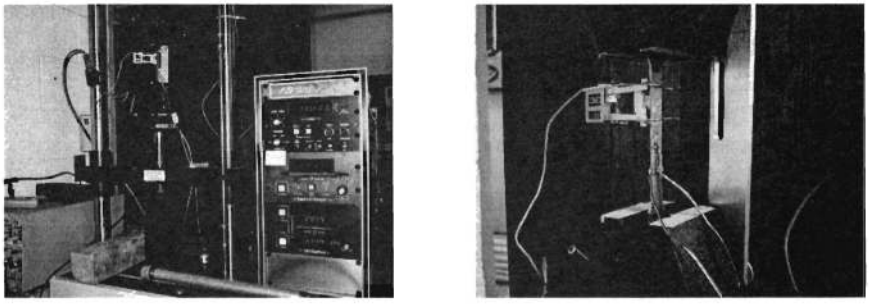

(a) Overall view of tension test setup (b) Details of tensile coupon with strain gages

Figure 14 Tension test setup

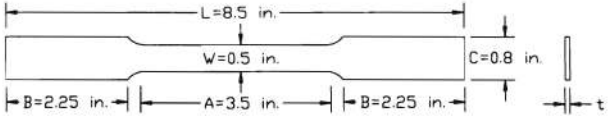

Figure 15 Dimensions of tensile coupon

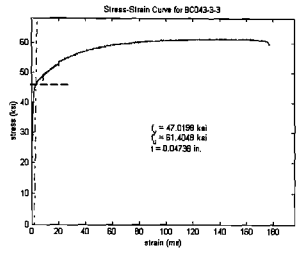

(a) Continuous yielding curve

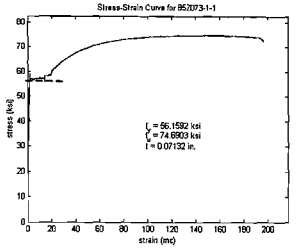

(b) Discontinuous yielding curve

Figure 16 Typical stress-strain curve of tensile test

Experimental Results

A summary of the local buckling test results is given in Table 4. Of the paired specimens in a test, the one denoted with an asterisk (*) is termed the "controlling specimen" because it has weaker capacity, as calculated by AISI (1996). The controlling specimens' data, selected from tests with expected configurations (gray items in Table 4), are used to examine the design methods.

The actuator load-displacement response is given in Figure 18, 19 and 20. Little non-linear response is observed prior to formation of the failure mechanism. The specimens, which have a tested capacity at or near the yield moment ($M_{test}/M_y \sim 1$), exhibit the most nonlinear deformation prior to failure; while the more slender specimens have essentially elastic response prior to formation of a sudden failure mechanism.

Failure of the weaker specimen, results in a significant loss in capacity. Redistribution of load into the second specimen of the pair causes failure soon thereafter. Failure of the second specimen can be recognized by the change in slope of the post-peak load-deformation response. In the studied members the post-peak response of the Cs was generally more gradual than comparable Zs, even in the thinner specimens. In tests on the Cs both specimens tend to fail at approximately the same time, as opposed to the progressive failure observed in most Zs. The observed failure mechanisms for the Cs are shown in Figure 23 (see Figure 22 for the Zs). The failure mechanism of the Cs is similar, but not identical to the Zs.

Strain gages were placed at midspan, on the lip and the top of the web, at the same vertical cross-section height, on nine C members, to monitor the longitudinal strain. Typical output from the gages is given in Figure 17. In the initial elastic range the gages read nearly identical and agree with simple beam theory predictions, indicating that the testing arrangement is achieving the desired loading about the geometric axis and no twisting is developing in the section. At an intermediate load level, before buckling deformations were visible, strain on either the lip or web began to reverse. In most, but not all, the strain on the lip began to reverse prior to the web. Once buckling initiates the strain distribution varies around the profile and along the length, and it becomes difficult to provide definitive conclusions from the limited strain data.

Table 3 Summary of tension test results

specimen	t (in)	f_y (ksi)	f_u (ksi)	f_u/f_y ratio
Deck1	0.0182	101.24	104.21	103%
Deck2	0.0183	100.72	101.54	101%
8.5Z120-3	0.1183	61.34	84.27	137%
8.5Z120-2	0.1176	60.05	82.56	137%
8.5Z105-2	0.1038	68.84	91.30	133%
8.5Z105-1	0.1048	66.85	89.13	133%
8.5Z092-4	0.0901	57.36	72.30	126%
8.5Z092-2	0.0891	56.99	71.91	126%
8.5Z082-2	0.0804	58.10	74.04	127%
8.5Z082-1	0.0806	58.37	74.01	127%
8.5Z073-6	0.0720	54.02	72.63	134%
8.5Z073-5	0.0727	55.58	73.62	132%
8.5Z073-4	0.0715	56.15	74.68	133%
8.5Z073-3	0.0720	55.55	74.33	134%
8.5Z073-2	0.0720	54.78	73.15	134%
8.5Z073-1	0.0715	55.66	74.07	133%
8.5Z065-3	0.0644	53.52	68.86	129%
8.5Z065-1	0.0642	53.07	68.58	129%
8.5Z059-4	0.0595	58.63	80.89	138%
8.5Z059-3	0.0595	58.46	81.03	139%
8.5Z059-2	0.0590	59.10	80.83	137%
8.5Z059-1	0.0590	58.90	80.58	137%
8C097-3	0.0936	59.64	76.12	128%
8C097-2	0.0978	59.89	76.69	128%
8C068-5	0.0755	48.58	64.58	133%
8C068-4	0.0768	53.05	66.25	125%
8C068-2	0.0753	51.43	65.95	128%
8C068-1	0.0757	51.75	65.34	126%
8C054-8	0.0540	40.35	52.75	131%
8C054-4	0.0591	46.61	60.95	131%
8C054-1	0.0545	40.04	52.05	130%
8C043-6	0.0491	45.04	60.78	135%
8C043-5	0.0496	44.85	60.97	136%
8C043-3	0.0472	45.96	61.48	134%
8C043-1	0.0475	45.68	61.33	134%
6C054-2	0.0616	36.10	50.33	139%
6C054-1	0.0616	36.96	50.01	135%
4C054-2	0.0561	44.71	54.54	122%
4C054-1	0.0551	44.97	55.49	123%
3.62C054-2	0.0554	31.98	54.11	169%
3.62C054-1	0.0555	32.77	53.91	165%
12C068-9	0.0652	35.08	58.50	167%
12C068-5	0.0654	34.86	58.63	168%
12C068-4	0.0670	57.28	75.93	133%
12C068-3	0.0671	56.64	74.90	132%
10C068-2	0.0572	33.56	57.32	171%
10C068-1	0.0573	34.19	56.93	167%
11.5Z073-1	0.0695	66.82	84.55	127%
11.5Z073-2	0.0709	65.40	82.82	127%
11.5Z082-1	0.0838	60.43	79.92	132%
11.5Z082-2	0.0837	61.49	81.00	132%
11.5Z092-1	0.1027	61.02	78.54	129%
11.5Z092-2	0.1033	60.42	78.00	129%

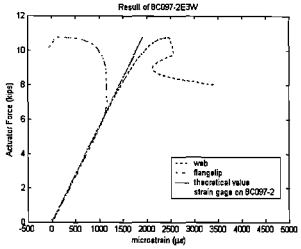

(a) t=0.097 in. (test 8C097-2E3W) first failure occurred in this specimen near the strain gages

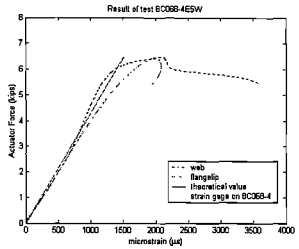

(b) t=0.068 in. (test 8C068-4E5W) first failure occurred in the other beam of the pair

Figure 17 Strain on web and lip for tests on 8 in. deep Cs

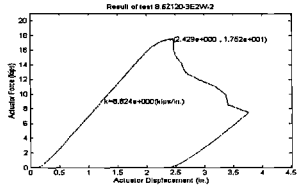

(a) t=0.120 in. (M_{test}/M_y=1.02)

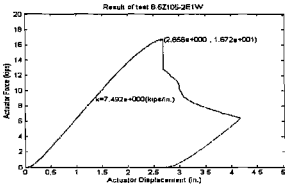

(b) t=0.105 in. (M_{test}/M_y=1.00)

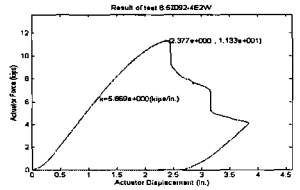

(c) t=0.092 in. (M_{test}/M_y=0.94)

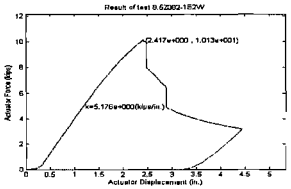

(d) t=0.082 in. (M_{test}/M_y=0.94)

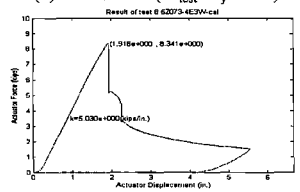

(e) t=0.073 in. (M_{test}/M_y=0.86)

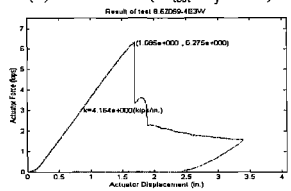

(f) t=0.059 in. (M_{test}/M_y=0.79)

Figure 18 Actuator force-displacement response for tests of 8.5 in. deep Zs

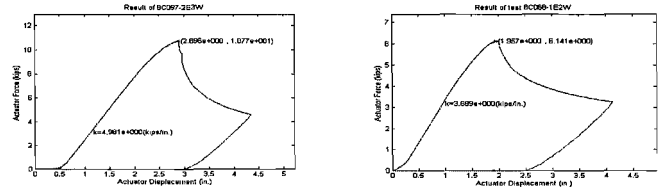

(a) t=0.097 in. (M_{test}/M_y=1.04) (b) t=0.068 in. (M_{test}/M_y=0.91)

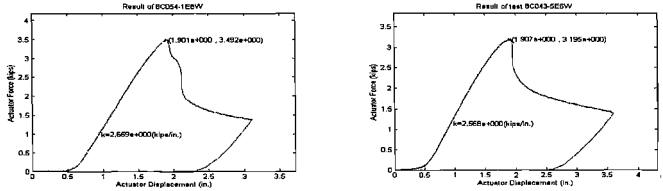

(c) t=0.054 in. (M_{test}/M_y=0.90) (d) t=0.043 in. (M_{test}/M_y=0.81)

Figure 19 Actuator force-displacement response for tests of 8 in. deep Cs

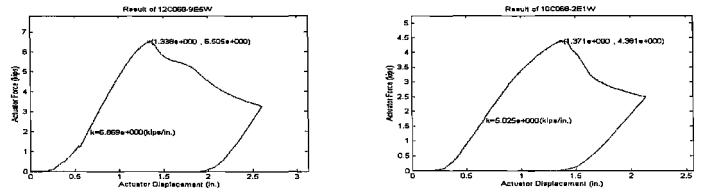

(a) h=12 in. (M_{test}/M_y=0.71) (b) h=10 in. (M_{test}/M_y=0.6)

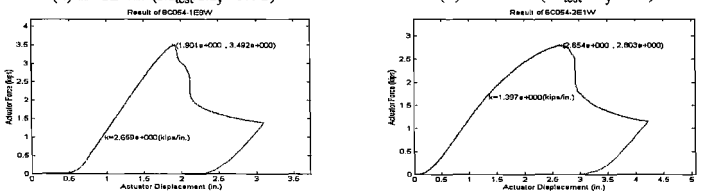

(c) h=8 in. (M_{test}/M_y=0.90) (d) h=6 in. (M_{test}/M_y=1.06)

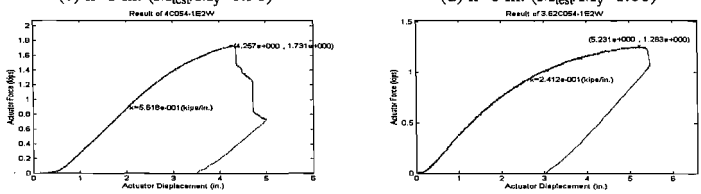

(e) h=4 in. (M_{test}/M_y=1.03) (f) h=3.62 in. (M_{test}/M_y=1.16)

Figure 20 Actuator force-displacement response for tests of 3.62 to 12 in. deep Cs

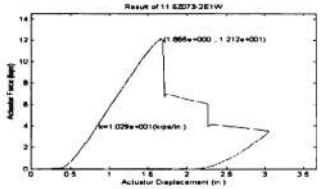

(a) t=0.073 in. (M_{test}/M_y=0.62)

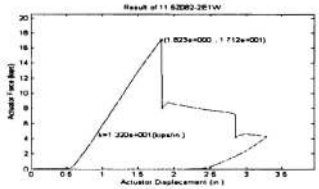

(b) t=0.082 in. (M_{test}/M_y=0.79)

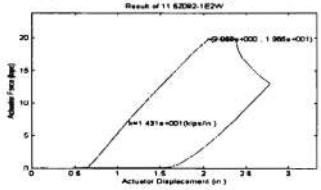

(c) t=0.092 in. (M_{test}/M_y=0.85)

Figure 21 Actuator force-displacement response for tests of 11.5 in. deep Zs

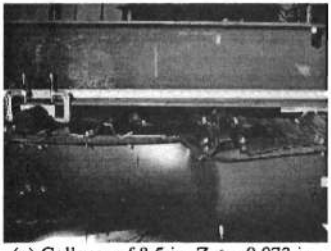

(a) Collapse of 8.5 in. Z, t = 0.073 in. (nominal)

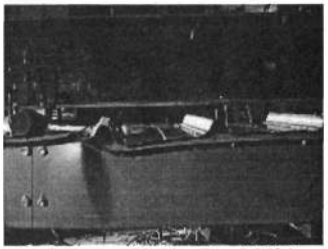

(b) Collapse of 8.5 in. Z, t=0.059 in. (nominal)

Figure 22 Collapses of 8.5 in. Zs t=0.073, 0.059 in.

(a) t=0.097 in (test 8C097-2E3W)

(b) t=0.043 in (test 8C043-5E6W)

Figure 23 Observed failure mechanisms for tests on 8 in. deep Cs

Table 4 Local buckling test results

Test label	Panel type	Specimen	M_{test}	M_y	M_{cr1}	M_{crd}	M_{test}/M_y	M_{test}/M_{aisi}	M_{test}/M_{S136}	$M_{test}/M_{NAS'01}$	M_{test}/M_{DS1}	M_{test}/M_{DSd}
8.5Z120-3E2W	C	8.5Z120-3	280.3	268	727	391	1.05	1.05	1.05	1.05	1.05	1.22
		8.5Z120-2 *	280.3	264	722	391	1.06	1.06	1.06	1.06	1.06	1.23
8.5Z105-2E1W	C	8.5Z105-2	267.5	270	480	293	0.99	1.05	1.07	1.04	0.99	1.28
		8.5Z105-1 *	251.2	252	479	292	1.00	1.00	1.07	1.04	1.00	1.28
8.5Z092-4E2W	C	8.5Z092-4	181.3	192	321	217	0.94	0.98	1.01	0.98	0.94	1.20
		8.5Z092-3 *	183.2	178	306	212	1.03	1.07	1.04	1.01	0.97	1.21
8.5Z082-1E2W	C	8.5Z082-1 *	162.1	174	226	170	0.93	1.00	1.05	1.00	1.01	1.25
		8.5Z082-2	162.1	174	229	174	0.93	1.00	1.05	0.99	1.00	1.24
8.5Z073-6E5W	A	8.5Z073-6 *	121.2	146	165	133	0.83	0.92	0.99	0.91	0.94	1.15
		8.5Z073-5	121.2	152	170	136	0.80	0.89	0.96	0.88	0.91	1.11
8.5Z073-4E3W	C	8.5Z073-4	133.5	151	161	129	0.88	0.98	1.06	0.98	1.02	1.26
		8.5Z073-3 *	133.5	150	165	135	0.89	1.00	1.08	0.99	1.01	1.24
8.5Z073-1E2W	B	8.5Z073-2 *	123.1	150	161	130	0.82	0.91	0.98	0.91	0.94	1.16
		8.5Z073-1	123.1	147	166	134	0.84	0.92	0.99	0.92	0.94	1.16
8.5Z065-3E1W	C	8.5Z065-3	95.5	125	115	90	0.77	0.86	0.96	0.86	0.93	1.18
		8.5Z065-1 *	95.5	122	176	137	0.78	0.88	0.99	0.88	0.93	1.19
8.5Z059-4E3W	C	8.5Z059-4 *	100.4	124	74	58	0.81	0.97	1.07	0.97	1.00	1.33
		8.5Z059-3	100.4	125	86	76	0.80	0.97	1.06	0.97	1.07	1.33
8.5Z059-2E1W	D	8.5Z059-2	98.9	127	86	74	0.78	0.96	1.04	0.96	1.04	1.32
		8.5Z059-1 *	98.9	127	86	74	0.78	0.96	1.04	0.96	1.04	1.32
8C097-2E3W	C	8C097-2 #	172.3	166	334	241	1.04	1.07	1.08	1.07	1.04	1.21
		8C097-3 *	172.3	165	338	245	1.04	1.06	1.08	1.07	1.03	1.20
8C068-4E5W	C	8C068-4 #	103.6	102	162	136	1.02	1.05	1.10	1.05	1.03	1.22
		8C068-5 *	103.6	114	176	146	0.91	0.95	0.99	0.95	0.93	1.10
8C068-1E2W	C	8C068-2 *	98.3	109	166	139	0.90	0.94	0.98	0.94	0.93	1.10
		8C068-1	98.3	108	165	137	0.91	0.94	0.98	0.94	0.94	1.11
8C054-1E8W	C	8C054-1 *#	59.2	66	65	54	0.90	0.96	1.07	0.96	1.04	1.25
		8C054-8	55.9	63	59	61	0.89	0.93	1.02	0.93	1.07	1.20
8C043-5E6W	C	8C043-5	51.1	64	47	51	0.80	0.95	1.04	0.95	1.05	1.17
		8C043-6 *	51.1	63	44	48	0.81	0.96	1.06	1.06	1.07	1.21
8C043-3E1W	C	8C043-3	47.8	63	41	45	0.76	0.93	1.01	0.93	1.03	1.17
		8C043-1 *#	47.8	62	41	44	0.77	0.94	1.01	0.93	1.04	1.18
12C068-9E5W	C	12C068-9 *	111.1	88	61	0.92	0.95	1.08	0.98	1.18	1.33
		12C068-5 #	104.1	110	90	122	0.95	0.98	1.12	1.12	1.19	1.33
12C068-3E4W	C	12C068-3	136.7	190	96	131	0.72	0.86	0.93	0.93	1.07	1.25
		12C068-4 *	136.7	192	94	121	0.71	0.90	0.97	0.95	1.07	1.28
10C068-2E1W	C	10C068-2	70.1	73	65	121	0.96	0.98	1.11	1.11	1.18	1.28
		10C068-1 *	71.1	77	65	113	0.92	0.96	1.06	1.06	1.14	1.28
6C054-2E1W	C	6C054-2 *#	45.8	43	101	87	1.06	1.06	1.09	1.06	1.06	1.14
		6C054-1	44.8	43	102	81	1.04	1.06	1.06	1.06	1.04	1.14
4C054-1E2W	D	4C054-1	27.7	27	66	43	1.02	1.11	1.11	1.10	1.02	1.15
		4C054-2 *#	27.7	27	73	45	1.03	1.13	1.13	1.11	1.03	1.15
3.62C054-1E2W	D	3.62C054-1 *#	20.2	17	64	38	1.16	1.20	1.20	1.20	1.16	1.24
		3.62C054-2	20.2	17	65	41	1.17	1.20	1.20	1.20	1.17	1.24
11.5Z092-1E2W!	C	11.5Z092-1	352.0	414	474	115	0.85	0.99	1.10	0.99	0.96	1.30
		11.5Z092-2 *	201.1	409	77	1	0.86	1.00	1.10	1.00	0.98	1.33
11.5Z082-2E1W	C	11.5Z082-2*	274.0	345	252	121	0.79	1.05	1.13	1.05	1.04	1.38
		11.5Z082-1	274.0	341	253	131	0.80	1.04	1.13	1.04	1.04	1.39
11.5Z073-2E1W	C	11.5Z073-2*	193.9	311	150	115	0.62	0.96	1.01	0.96	0.94	1.30
		11.5Z073-1#	193.9	315	144	122	0.62	0.96	1.00	0.96	0.95	1.30

Note:
Grey items are the final effective data.
!: Result is estimated due to peak load exceeds the recording range.
*: Controlling specimens
#: Strain gages were placed at midspan, on the lip and the top of the web, at the same vertical cross-section height
Panel fastener type:
A: one screw on the lapped side of raised corrugation
B: one screw on each side of raised corrugation
C: two screws on each side of raised corrugation in the constant moment region, one screw on each side of raised corrugation in the shear spans
D: two screws on each side of raised corrugation, and two screws in center of pans for the constant moment region, one screw on each side of raised corrugation in the shear span

Comparison with Design Methods

Four design methods were considered for comparison: the existing American Specification (AISI 1996), the existing Canadian Standard (S136 1994), the newly adopted combined U.S./Canada/Mexico - North American Specification (NAS 2001) and the recently proposed Direct Strength Method (Schafer and Peköz 1998, Schafer 2002a,b).

Test-to-predicted

The average (μ) and standard deviation (σ) of the test-to-predicted ratios indicate that overall, all considered methods provide an adequate prediction of the test data. The test-to-predicted ratios for AISI and S136 are graphically depicted in Figure 24. NAS results are close to AISI when h/b_c is less than 4; otherwise they will be close to S136 results. The AISI and S136 methods are identical except for the expressions for the effective width of the web. The S136 method assumes the web is partially effective for $\lambda_{web} > 0.673$ while the AISI method does not. The AISI has systematically higher predictions than S136 for the slender specimens. The average strength difference between the AISI and S136 predictions is 7%, with AISI having a test-to-predicted ratio slightly less than 1.0 and that of S136 greater than 1.0.

Table 4 and Table 5 present the summary statistics for the Direct Strength Method. Failures by local buckling (M_{DSl}) and by distortional buckling (M_{DSd}) are both considered. The high test-to-predicted ratios for the distortional buckling strength (M_{test}/M_{DSd}) indicate that distortional buckling is successfully restricted with the testing details employed. Further, it indicates that without the fastener details in place the expected strength would be significantly reduced.

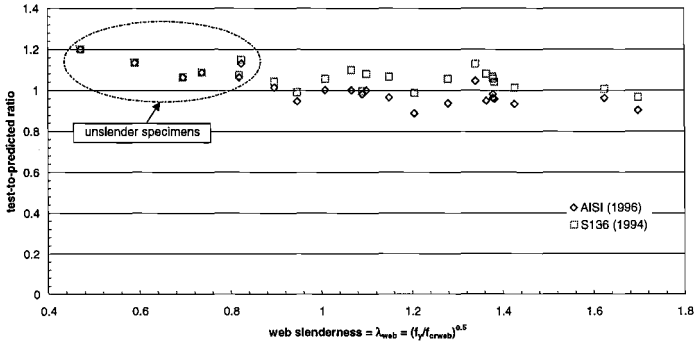

Figure 24 Test-to-predicted ratios vs. web slenderness for slender specimens

Table 5 Summary of test-to-predicted ratios for existing and proposed design methods

		μ					σ				
		M_{test}/M_{AISI}	M_{test}/M_{S136}	M_{test}/M_{NAS}	M_{test}/M_{DS1}	M_{test}/M_{DSd}	M_{test}/M_{AISI}	M_{test}/M_{S136}	M_{test}/M_{NAS}	M_{test}/M_{DS1}	M_{test}/M_{DSd}
Unslender N=6	Controlling	1.11	1.12	1.11	1.07	1.22	0.05	0.05	0.05	0.05	0.06
	Second	1.09	1.09	1.09	1.05	1.21	0.06	0.06	0.06	0.06	0.05
Slender N=15	Controlling	0.97	1.04	0.98	1.02	1.25	0.04	0.04	0.05	0.07	0.08
	Second	0.96	1.04	0.98	1.03	1.25	0.05	0.06	0.07	0.07	0.08

Note:
Slender: the specimens with $M_{test}/M_y<1.0$ (total N=15 tests)
Unslender: the specimens with $M_{test}/M_y>=1.0$ (total N=6 tests)
Controlling: the controlling specimen
Second: the uncontrolling specimen of the paired set
M_{AISI}: AISI (1996) predicted flexural capacity
M_{S136}: S136 (1994) predicted flexural capacity
M_{NAS}: NAS (2001) predicted flexural capacity
M_{DS1}: Direct Strength - Local mode expression as reported in (2002b) to AISI (a.k.a: M_{n1})
M_{DSd}: Direct Strength - Distortional mode expression as reported in (2002b) to AISI (a.k.a: M_{nd})

Web Effective Width

If we assume that the flange expressions are accurate, then we can use the experimentally observed capacity to back-calculate the correct effective width for the web, expressed as $(b_1+b_2)/b_{comp}$, where b_1 and b_2 are the effective width of the compressive portions of the web, and b_{comp} is the depth of the full compression portion of the web. The results of this calculation are given in Figure 25.

The majority of the bending strength is derived from the flange. Therefore, large changes are required in the web effective width in order to make a small change in the predicted bending capacity. For example, the AISI prediction for 8.5Z059-1, λ_{web}=1.38, M_{test}/M_{aisi} = 96%, the predicted web effectiveness by AISI is 88% and the back-calculated experimental web effectiveness is 69% – a 19% difference! Therefore, the large differences between the two methods tend to get overstated when examining the web effective width in isolation, as in Figure 25.

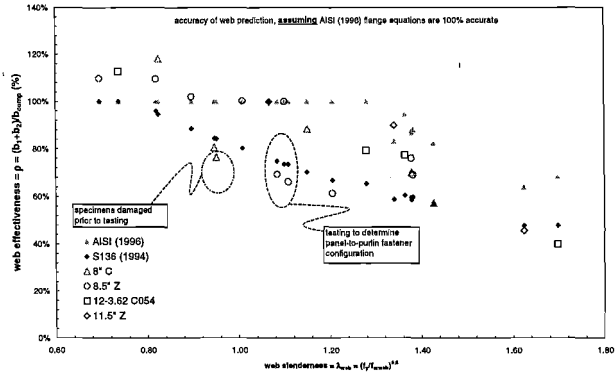

Figure 25 Back-calculated experimental web effective width vs. predictions

Conclusions

Through computational and experimental means the developed testing plan and details have been shown to adequately restrict distortional buckling and provide a simple repeatable test that generates the local buckling flexural capacity for C- and Z-Sections. Overall the test results indicate that AISI (1996), S136 (1994), and the new NAS (2001) design methods provide adequate strength predictions. However, this overall agreement is primarily due to conservative predictions in unslender members that had observable inelastic reserve capacity ($M_{test}/M_y>1$). Among the considered methods, the Direct Strength method provides the best test-to-predicted ratio for both slender and unslender specimens. The test results demonstrate that many improvements in the elastic buckling and effective width calculation of Cs and Zs are still possible. The authors intend to pursue additional testing and analysis to determine the distortional buckling capacity of Cs and Zs as well as more closely define the role of fasteners and other details.

Acknowledgement

The sponsorship of AISI and MBMA and the donation of materials by Varco-Pruden, and Clark Steel is gratefully acknowledged. The assistance of the AISI task group in developing the testing plan is appreciated. Don Johnson, Maury Golovin, Joe Nunnery, Joe Wellinghoff, and Steve Thomas have all been helpful with their ideas and generous with their time. Johns Hopkins undergraduates: Sam Phillips, Liakos Ariston, and Andrew Myers have provided additional support in the lab and deserve recognition as well. The assistance of Jack Spangler in re-invigorating the JHU structural testing facility has been invaluable. The donation of steel parts by Prosser Steel is also appreciated.

References

AISI (1996). "Specification for the Design of Cold-Formed Steel Structural Members." American Iron and Steel Institute. Washington, D.C.

NAS (2001) "OCTOBER 12, 2001 DRAFT of North American Specification for the Design of Cold-Formed Steel Structural Members." American Iron and Steel Institute. Washington, D.C.

S136 (1994) "Cold-Formed Steel Structural Members" S136-94. Canadian Standards Association. Rexdale, Ontario, Canada

Schafer, B.W. (2002a) "Local, Distortional, and Euler Buckling in Thin-walled Columns." *J. of Struct. Eng.* ASCE. 128(3) 289-299.

Schafer, B.W. (2002b) "Design Manual for Direct Strength Method of Cold-Formed Steel Design." Report to the American Iron and Steel Institute, Washington, D.C. (available online at www.ce.jhu.edu/bschafer/direct_strength)

Schafer, B.W., Peköz, T. (1998). "Direct Strength Prediction of Cold-Formed Steel Members using Numerical Elastic Buckling Solutions." *14th Int'l. Spec. Conf. on Cold-Formed Steel Structures*. St. Louis, Missouri.

Schafer, B.W., Peköz, T. (1999). "Laterally Braced Cold-Formed Steel Flexural Members with Edge Stiffened Flanges." *J. of Struct. Eng.* ASCE. 125(2) 118-127.